ISSN Online: 2821-1693

Transactions on Machine Intelligence

Journal Homepage: https://tmachineintelligence.ir/index.php/TMI

Thermal Management of Insulated-Gate Bipolar Transistor Modules by Air and Liquid Cooling: A Numerical Study

A. Soleimani[1], A. Moghoufe[2], M. Saffaripour[3,*]

[1] School of Mechanical Engineering, College of Engineering, University of Tehran, Iran
[2] School of Mechanical Engineering, College of Engineering, University of Tehran, Iran
[3] School of Mechanical Engineering, College of Engineering, University of Tehran, Iran

ARTICLE INFO

Article History:
Received 16 November 2023
Received in revised form 22 January 2024
Accepted 5 March 2024
Available online 7 March 2024

Keywords:
IGBT Thermal Management, Air-Cooled Heat Sink, Liquid-Cooled Cold Plate, Computational Fluid Dynamics

ABSTRACT

Thermal management of three insulated-gate bipolar transistor (IGBT) modules with application in power inverters is studied numerically with two different cooling approaches, an air-cooled heat sink and a liquid-cooled cold plate. Four air-cooled heat sink configurations have been studied and compared: a natural-convection configuration, a forced parallel-flow configuration, and two forced impingement-flow configurations with different fans. For the cold plate, a suitable coolant is chosen based on the operating conditions of the current study. The maximum total heat dissipation rate of the three IGBT modules, which includes switching and conductive power dissipation rates, is calculated to be 1200 W at peak load. The air-cooled and liquid-cooled cases are studied under a variety of operating conditions, including different ambient temperatures and heat dissipation rates. The results show that natural convection can only be used for total heat dissipation rates below 300 W. Whereas, the forced impingement-flow air cooling configuration with large fans and the liquid cooling configuration can keep the junction temperature of the IGBTs below the maximum permissible value under all the operating conditions used in this study. The liquid-cooled cold plate has the lowest thermal resistance and because of retaining the largest safety margin for junction temperature, this method is suitable for power dissipation rates higher than 1200 W. The results indicate that the performance of the air-cooled heat sinks is not a strong function of air flow direction and mainly depends on air flow rate.

1. INTRODUCTION

Power electronic devices are widely used in applications such as power plants, consumer electronics, power supplies, and electric vehicles. These devices often generate significant heat, which can raise their operating temperatures beyond permissible limits. One such device is the insulated-gate bipolar transistor (IGBT), commonly employed as an electronic switch in power inverters and converters. The IGBT junction, located at the interface of its collector layers, is where electrical current flows and heat is dissipated. This junction is typically the hottest part of the IGBT, and overheating can lead to thermal breakdown and device failure. Consequently, effective thermal management techniques are essential to ensure the optimal performance and longevity of IGBT modules.

* Corresponding Author: m.saffaripour@ut.ac.ir
School of Mechanical Engineering, College of Engineering, University of Tehran, Iran

http://dx.doi.org/10.47176/TMI.2024.11

The use of heat sinks cooled by natural air convection is a traditional and cost-effective method for electronics cooling. This approach leverages air, a readily available and free coolant. Heat sinks designed for forced air convection are used with two flow configurations: impingement flow and parallel flow. In the impingement-flow setup, air flows perpendicular to the heat sink base, while in the parallel-flow setup, air flows along the heat sink base, with fins aligned to create multiple air channels.

However, air cooling is generally insufficient for high-power electronic devices, necessitating the use of liquid cooling in such cases. Liquids, with their superior thermal conductivity and heat capacity compared to gases, can handle higher heat dissipation rates. Liquid cooling is typically implemented using cold plates, which are heat sinks that circulate liquid coolant instead of air.

In this study, the thermal performance of air- and liquid-cooling methods for managing the heat of three IGBT modules is analyzed through numerical simulations. The air-cooled heat sinks are evaluated using one natural-convection configuration and three forced-convection configurations: one parallel-flow and two impingement-flow setups. For liquid cooling, a simple and cost-effective formed-tube cold plate is simulated. The thermal properties of various coolants are examined, and the most suitable coolant for the study's operating conditions is selected. To establish the optimal application range for each cooling method, their thermal performance is assessed under varying conditions of heat dissipation rates and ambient temperatures.

2. METHODOLOGY

2.1. Heat Dissipation

In the present study, each IGBT module is supposed to dissipate heat at a rate of 400 W during its peak-load operation.

2.2. Governing Equations

The model solves the Favre-averaged three-dimensional conservation equations of mass, momentum, and energy in order to obtain the mean turbulent flow of a selected liquid coolant and air which characterizes fairly an ideal gas [1, 2]. The conservation equations of mass, momentum, and energy are formulated respectively in Eq. (1), (2), and (3):

$$\vec{\nabla} \cdot (\bar{\rho}\tilde{\vec{U}}) = 0 \tag{1}$$

$$\vec{\nabla} \cdot (\bar{\rho}\tilde{\vec{U}}[\tilde{U}]) = -[\nabla]\bar{P} + \vec{\nabla} \cdot ([\bar{\tau}] - [R]) + \bar{\rho}[g] \tag{2}$$

$$\vec{\nabla} \cdot (\bar{\rho}\tilde{\vec{U}}\tilde{h}_s) = \overline{\vec{U} \cdot \vec{\nabla}P} + \vec{\nabla} \cdot (\kappa\vec{\nabla}T - \overline{\rho\vec{U}''h_s''}) + \bar{\Phi} + \bar{\dot{q}} \tag{3}$$

where $\bar{\rho}$, $\tilde{\vec{U}}$, $\bar{P}$, and $\tilde{h}_s$are Reynolds-averaged density, Favre-averaged velocity vector, Reynolds-averaged pressure, and Favre-averaged specific sensible enthalpy respectively. Operator $[\nabla]$is a matrix operator and is formulated as Eq. (4) in Cartesian coordinates. $[\bar{\tau}]$ represents mean viscous stress and subsequently, $[R]$ denotes Reynolds stress. These two terms are formulated in Cartesian coordinates by Eq. (5) and (6) respectively. The concept of viscous stress tensor for Newtonian fluid is concisely discussed in any accessible fluid-mechanics reference book, therefore, any unnecessary explanation with regard to that is avoided.

$$[\nabla] = \begin{bmatrix} \partial/\partial x \\ \partial/\partial y \\ \partial/\partial z \end{bmatrix} \tag{4}$$

$$[\bar{\tau}] = \begin{bmatrix} \bar{\tau}_{xx} & \bar{\tau}_{xy} & \bar{\tau}_{xz} \\ \bar{\tau}_{xy} & \bar{\tau}_{yy} & \bar{\tau}_{yz} \\ \bar{\tau}_{xz} & \bar{\tau}_{yz} & \bar{\tau}_{zz} \end{bmatrix} \begin{bmatrix} \hat{\imath} \\ \hat{\jmath} \\ \hat{k} \end{bmatrix} = \begin{bmatrix} \bar{\tau}_{xx}\hat{\imath} + \bar{\tau}_{xy}\hat{\jmath} + \bar{\tau}_{xz}\hat{k} \\ \bar{\tau}_{xy}\hat{\imath} + \bar{\tau}_{yy}\hat{\jmath} + \bar{\tau}_{yz}\hat{k} \\ \bar{\tau}_{xz}\hat{\imath} + \bar{\tau}_{yz}\hat{\jmath} + \bar{\tau}_{zz}\hat{k} \end{bmatrix} \tag{5}$$

$$[R] = \begin{bmatrix} \overline{\rho u'' u''}\hat{\imath} + \overline{\rho v'' u''}\hat{\jmath} + \overline{\rho w'' u''}\hat{k} \\ \overline{\rho u'' v''}\hat{\imath} + \overline{\rho v'' v''}\hat{\jmath} + \overline{\rho w'' v''}\hat{k} \\ \overline{\rho u'' w''}\hat{\imath} + \overline{\rho v'' w''}\hat{\jmath} + \overline{\rho w'' w''}\hat{k} \end{bmatrix} \tag{6}$$

Furthermore, $[g]$, $\bar{\Phi}$, and $\bar{\dot{q}}$ refer to matrix of gravitational acceleration, viscous dissipation function, and volumetric heat source correspondingly. Note that $[\tilde{U}]$ is the matrix notation of Favre-averaged velocity. Eq. (7) defines this matrix in Cartesian coordinates and explains how three distinct equations are extracted from the conservation of momentum. Matrices are able to generate three distinct momentum equations which correspond to three orthogonal directions. It is also worth mentioning that for solving energy equation in solids, the convective terms of the equation are set to zero.

$$[\tilde{U}] = \begin{bmatrix} \tilde{u} \\ \tilde{v} \\ \tilde{w} \end{bmatrix} \Rightarrow \bar{\rho}\vec{\tilde{U}}[\tilde{U}] = \begin{bmatrix} \bar{\rho}\vec{\tilde{U}}\tilde{u} \\ \bar{\rho}\vec{\tilde{U}}\tilde{v} \\ \bar{\rho}\vec{\tilde{U}}\tilde{w} \end{bmatrix} = \begin{bmatrix} \bar{\rho}\tilde{u}\tilde{u}\hat{\imath} + \bar{\rho}\tilde{v}\tilde{u}\hat{\jmath} + \bar{\rho}\tilde{w}\tilde{u}\hat{k} \\ \bar{\rho}\tilde{u}\tilde{v}\hat{\imath} + \bar{\rho}\tilde{v}\tilde{v}\hat{\jmath} + \bar{\rho}\tilde{w}\tilde{v}\hat{k} \\ \bar{\rho}\tilde{u}\tilde{w}\hat{\imath} + \bar{\rho}\tilde{v}\tilde{w}\hat{\jmath} + \bar{\rho}\tilde{w}\tilde{w}\hat{k} \end{bmatrix} \tag{7}$$

Some terms such as $[R]$, $\overline{\rho\vec{U}''h_s''}$, $\overline{\vec{U}\cdot\vec{\nabla}P}$, and $\bar{\Phi}$ which were introduced previously in Eq. (1), (2), and (3) should be modeled or neglected, if possible, otherwise they cause closure problem. There are several mathematical models which are capable of estimating these terms in presence of turbulence. For example, $\overline{\rho u'' v''}$, a Reynolds-stress component includes fluctuating velocity variables which emerge after the procedure of Reynolds decomposition and Reynolds averaging. Fluctuating variables are not supposed to be resolved and Boussinesq's hypothesis is an acceptable option for modeling $\overline{\rho u'' v''}$ according to Eq. (8). $\overline{\rho\vec{U}''h_s''}$ known as turbulent enthalpy flux can also be modeled by Boussinesq's hypothesis and Reynolds analogy according to Eq. (9):

$$\overline{\rho u'' v''} = -\mu_t\left(\frac{\partial\tilde{u}}{\partial y} + \frac{\partial\tilde{v}}{\partial x}\right) + \frac{2}{3}\mu_t\left(\frac{\partial\tilde{u}}{\partial x} + \frac{\partial\tilde{v}}{\partial y} + \frac{\partial\tilde{w}}{\partial z}\right) + \frac{2}{3}\bar{\rho}k \tag{8}$$

$$\overline{\rho\vec{U}''h_s''} = -\frac{\mu_t C_p}{Pr_t}\vec{\nabla}\tilde{T} \tag{9}$$

where μ_t and $\mathrm{Pr_t}$ are turbulent viscosity and turbulent Prandtl number (which is a constant) respectively. The k-ε model [3] along with enhanced wall treatment [4] are selected to model turbulent flow. The equations for turbulent kinetic energy (k) and its dissipation rate (ε) are formulated as Eq. (10) and (11) [5]:

$$\vec{\nabla}\cdot(\bar{\rho}k\vec{\tilde{U}}) = \vec{\nabla}\cdot\left((\mu + \frac{\mu_t}{\sigma_k})\vec{\nabla}k\right) + G_k + \bar{\rho}\varepsilon \tag{10}$$

$$\vec{\nabla}\cdot(\bar{\rho}\varepsilon\vec{\tilde{U}}) = \vec{\nabla}\cdot\left((\mu + \frac{\mu_t}{\sigma_\varepsilon})\vec{\nabla}\varepsilon\right) + C_{1\varepsilon}\frac{\varepsilon}{k}G_k - C_{2\varepsilon}\bar{\rho}\frac{\varepsilon^2}{k} \tag{11}$$

where G_k is turbulence kinetic energy generation due to the average velocity gradients, μ is dynamic viscosity, $C_{1\varepsilon}$ and $C_{2\varepsilon}$ are constants. σ_k and σ_ε are turbulent Prandtl numbers for k and ε respectively. Ultimately, k-ε model calculates the flow variable μ_t using Eq. (12):

$$\mu_t = \bar{\rho}C_\mu\frac{k^2}{\varepsilon} \tag{12}$$

where C_μ is a constant equal to 0.09 for k-ε model. Thermal resistance of heat sink, R_{th}, is defined to evaluate the thermal performance of heat sinks in order to be compared to the values reported in the literature for other heatsinks. Eq. (13) is the definition of thermal resistance [6]:

$$R_{th} = \frac{\Delta T}{\bar{\dot{Q}}} \tag{13}$$

where ΔT is the difference between the mean base temperature of heat sink and the temperature of inlet fluid, and $\bar{\dot{Q}}$ is the mean heat transfer rate from the heat sink base to the fluid. The mean junction temperature of the IGBT, T_J, is calculated by Eq. (14) using the thermal resistance of heat sink:

$$T_J = T_s + R_{th}{}^{(J-C)}\bar{Q} \tag{14}$$

where T_s is the mean temperature at the heat sink-IGBT interface, and the $R_{th}{}^{(J-C)}$ is the thermal resistance between heat sink base and the junction whose value is reported by IGBT manufacturer. For the LWH300G1201 IGBT, $R_{th}{}^{(J-C)}$ is 0.07°C/W and the maximum permissible junction temperature is 125°C [2]. The inlet Reynolds number of air and liquid flows are derived using the Eq. (15):

$$Re_{in} = \frac{\bar{\rho}_{in} U_{in} d}{\mu} \tag{15}$$

where $\bar{\rho}_{in}$, U_{in}, and d are mean inlet density, inlet velocity, and inlet hydraulic diameter of the fluid flow respectively.

2.3. Numerical Model

In this study, ANSYS Fluent version 18.2 [4] is used to perform simulations by solving three-dimensional governing equations. The software employs the finite volume method (FVM) to discretize the equations and solve them across the computational domain. The inlet Reynolds numbers for the airflow exceed 100,000, while those for the liquid flow are greater than 3,000, indicating fully turbulent flow in all simulations. Radiation heat transfer is negligible at the operating temperatures considered in this study and is therefore excluded. Initial conditions assume zero velocity for the fluids and ambient temperature throughout the domain. Convergence criteria are set to 10−610^{-6} for the energy equation and 10−410^{-4} for the continuity and momentum equations. The computational mesh is composed of tetrahedron, wedge, and pyramid cell types, with an average skewness value of 0.2.

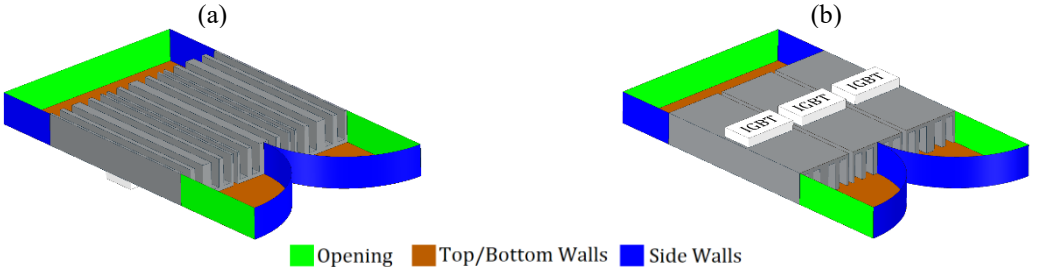

Fig. 1. Schematic views of the air-cooled heat sink and its casing, showing (a) the air flow passage through the casing and over the heat sink, and (b) the bottom of the heat sink where the IGBTs are attached.

2.4. Geometry and Boundary Conditions

2.4.1. Air Cooling:

The air-cooled heat sink analyzed in this study is modeled after an existing design used in a power inverter. Figures 1(a) and 1(b) provide schematics of the heat sink and its casing, with all casing boundaries labeled. The casing features three openings to facilitate airflow over the heat sink. The heat sink consists of three identical segments, arranged parallel to each other with a 10 mm gap between them. The fin thickness varies among the segments, and the overall length of the heat sink is 40 cm. Each segment's base center is attached to an IGBT module, as depicted in Fig. 1(b). The interface between each IGBT module and the heat sink is a rectangular area measuring 108 mm in length and 62 mm in width [2]. The heat sink is made of aluminum, which has a thermal conductivity of 210 W/mK.

As previously mentioned, three airflow modes can be utilized for cooling the heat sink: natural convection, forced convection with parallel flow, and forced convection with impingement flow. Four specific configurations enabling these cooling methods are illustrated in Fig. 2:

1. **Natural Convection (Fig. 2a):** The inverter casing is positioned vertically, allowing buoyancy-driven airflow. Air enters the casing through the bottom opening and exits through openings on the upper side walls.
2. **Forced Convection with Parallel Flow (Fig. 2b):** Four 60-mm-diameter fans, evenly spaced, are installed at the casing's front opening (highlighted in yellow) to direct airflow over the heat sink. The air exits through downstream openings.
3. **Forced Convection with Impingement Flow (Figs. 2c and 2d):**
    - Configuration 1 (Fig. 2c): Four 60-mm-diameter fans, evenly spaced, are placed above the heat sink.
    - Configuration 2 (Fig. 2d): Three 120-mm-diameter fans, evenly spaced, are positioned above the heat sink.

In both impingement flow setups, the incoming air jets strike the heat sink directly, flow across the fins, and exit through the three designated openings.

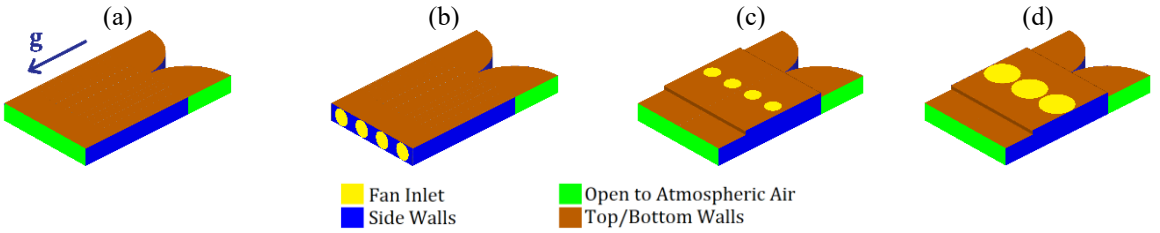

Fig. 2. The air-cooling configurations under study: (a) natural-convection configuration, (b) forced-convection configuration with parallel flow, (c) forced-convection with impingement flow and 60-mm fans, and (d) forced-convection with impingement flow and 120-mm fans.

As illustrated in Fig. 2, all air-cooling configurations exhibit geometric symmetry. To minimize computational costs, only half of each configuration's geometry is modeled as the computational domain. A symmetry boundary condition is applied along the plane dividing the omitted half. A constant heat flux boundary condition is imposed on the surfaces where the IGBTs are mounted. Since only half of the geometry is simulated, the heat sources represent the heat dissipation from 1.5 IGBT modules. The heat dissipation rate for each module ranges from 100 to 400 W, allowing evaluation of thermal performance under varying loads, with the maximum rate of 400 W corresponding to peak load conditions.

At the inlet, boundary conditions include a constant volumetric flow rate and constant temperature equal to the ambient temperature, which varies from 0°C to 45°C to simulate seasonal changes. Atmospheric pressure is assumed at the outlets. For the casing walls, a heat flux boundary condition with a constant convection coefficient of 10 W/m^2K is applied to account for natural convection heat transfer to the ambient air.

This study uses two fans commonly employed in electronics cooling: a 60-mm-diameter fan and a 120-mm-diameter fan, both manufactured by San Ace [7]. Fan performance curves, which depict fan pressure rise as a function of volumetric flow rate, are used to determine the operating flow rate of the fans. Figures 3(a–c) show these curves, along with the calculated pressure drop of the heat sink as a function of flow rate for the three forced-convection configurations. The operating flow rate of each fan is determined at the intersection of the fan performance curve and the heat sink pressure drop curve, marked with dashed red lines in the figures. The operating flow rates are 1.14 m^3/min for the parallel-flow configuration, 1.20 m^3/min for the impingement-flow configuration with 60-mm fans, and 6.87 m^3/min for the impingement-flow configuration with 120-mm fans.

Because smaller fans are used in the parallel-flow configuration, its operating flow rate is lower than that of the impingement-flow configurations. This highlights the impact of fan size on airflow performance in forced-convection cooling setups.

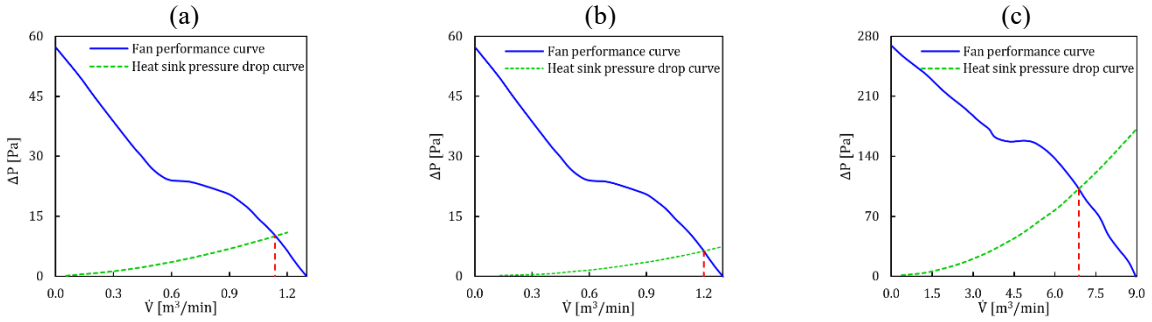

Fig. 3. Fan pressure rise as a function of volumetric flow rate, labeled as fan performance curve, and heat sink pressure drop as a function of volumetric flow rate, labeled as heat sink pressure drop curve, for (a) the parallel-flow configuration, (b) the impingement-flow configuration with 60-mm fans, and (c) the impingement-flow configuration with 120-mm fans. The operating flow rate for each configuration, identified with the dashed red lines, is obtained by intersecting the fan performance curve and the heat sink pressure drop curve.

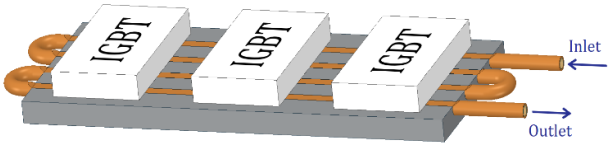

Fig. 4. A schematic drawing of the four-pass cold plate modeled in the present work with three attached IGBT modules.

2.4.2. Liquid Cooling

This study models an affordable and easy-to-manufacture four-pass formed-tube cold plate, schematically shown in Fig. 4. The design is based on the 416601U0000G cold plate manufactured by AAVID Company [8]. The cold plate consists of a copper tube embedded within an aluminum plate, with the tube flattened to enhance thermal contact with the heat source. The aluminum plate measures 305 mm in length, 127 mm in width, and 15.2 mm in thickness. The copper tube has an inner diameter of 7.02 mm and an outer diameter of 9.5 mm. The three IGBT modules are symmetrically mounted on the cold plate with equal 40-mm spacing between them, following the actual cold plate's reported dimensions. The thermal conductivity values for aluminum and copper are 210 W/mK and 385 W/mK, respectively.

The boundary and operating conditions for the cold plate are analogous to those used in the air-cooled configurations. A constant heat flux boundary condition is applied at the IGBT-cold plate interfaces, with heat flux ranging from 100 to 400 W per IGBT. Outer surfaces of the cold plate are modeled with a constant heat flux boundary condition representing natural convection to ambient air, with a convection coefficient of 10 W/m²K. Longitudinal heat conduction in the copper tubing is neglected due to the thinness of its walls. The coolant inlet temperature matches the ambient temperature, which varies between 0°C and 45°C. According to the manufacturer's specifications, the maximum coolant mass flow rate for the 416601U0000G cold plate is 6.0 kg/min (1.5 GPM) [8]. In this study, the coolant mass flow rate is varied between 1.5 kg/min and 6.0 kg/min.

2.5. Mesh Independency

The goal of the mesh independency analysis is to determine the optimal mesh size, balancing computational cost and resolution accuracy. Simulations are performed using different mesh sizes, defined by the number of cells, for both air-cooled and liquid-cooled configurations.

For the air-cooled heat sink with the parallel-flow forced-convection configuration, Fig. 5(a) illustrates the calculated pressure drop as a function of mesh size. The pressure drop stabilizes for mesh sizes exceeding 646,800 cells, indicating mesh independence. Consequently, all air-cooling simulations use a mesh with 646,800 cells.

For the cold plate, Fig. 5(b) presents the computed pressure drop for varying mesh sizes. The pressure drop shows negligible changes when using more than 527,000 cells. Therefore, a mesh with 527,000 cells is determined to be optimal for the cold plate simulations.

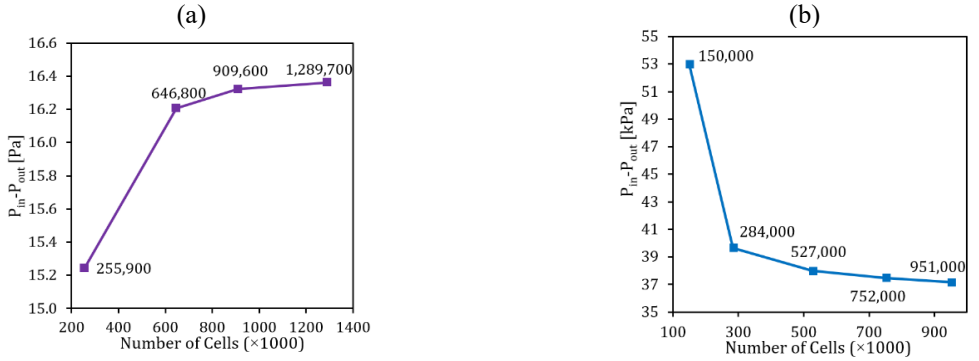

Fig. 5. The effect of changing mesh size, quantified by the number of cells used in the mesh, on the computed pressure drop for (a) the air-cooled heat sink, and (b) the cold plate.

3. RESULTS AND DISCUSSION

In this study, the thermal performance of an air-cooled heat sink and a liquid-cooled cold plate are investigated under different operating conditions. A summary of the studied configurations is presented in Table 2.

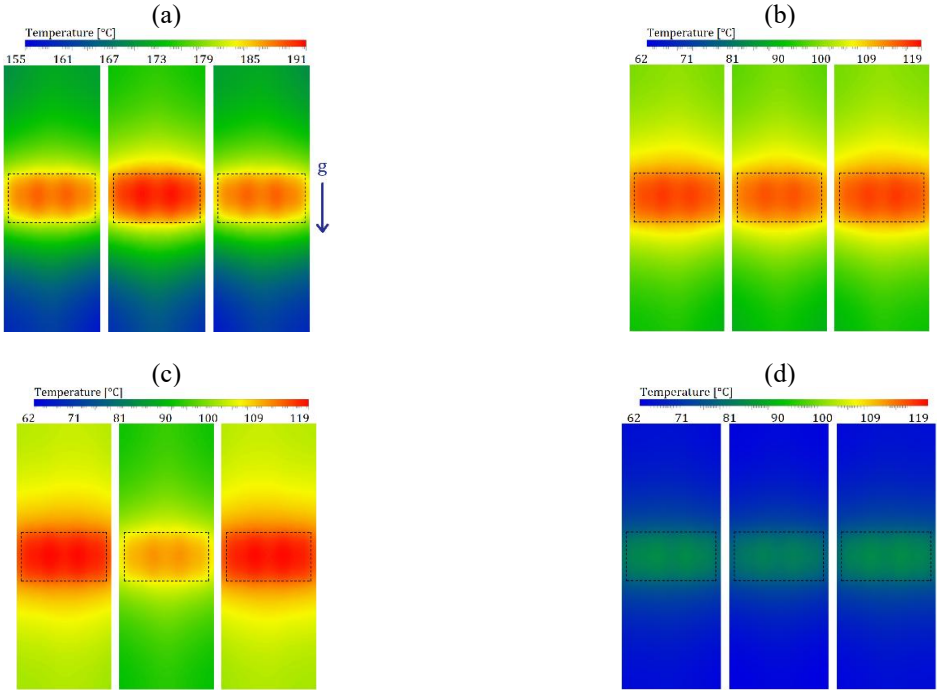

Fig. 6. Temperature distribution over the heat sink base for (a) natural-convection, (b) forced-convection with parallel-flow, (c) forced-convection with impingement-flow and 60-mm fans, and (d) forced-convection with impingement-flow and 120-mm fans.

Table 2. A summary of the cooling configurations studied for the thermal management of three IGBT modules.

Cooling Method	Cooling Device	Coolant	Ambient Temperature [°C]	Total Heat Dissipation Rate [W]
Natural Convection	Heat Sink	Air	0-45	300-1200
Forced Parallel-Flow with 60-mm Fans	Heat Sink	Air	0-45	300-1200
Forced Impingement Flow with 60-mm Fans	Heat Sink	Air	0-45	300-1200
Forced Impingement Flow with 120-mm Fans	Heat Sink	Air	0-45	300-1200
Liquid Cooling [$\dot{m}$ = 1.5–6.0 kg/min]	Cold Plate	Water-Ethylene Glycol Solution	0-45	300-1200

3.1 Air Cooling

Temperature distributions on the heat sink base for various air-cooling configurations are illustrated in Figs. 6(a–d). These include natural convection, parallel-flow forced convection, and impingement-flow forced convection with 60-mm and 120-mm fans, respectively. The simulations are conducted using an ambient air temperature of 45°C and a total heat dissipation rate of 900 W, with the locations of the IGBT modules marked by dashed lines.

Natural convection produces the highest base temperatures, with a peak of approximately 191°C, due to the laminar airflow resulting in low heat transfer efficiency. A significant temperature gradient is observed, with the lower portion of the heat sink being cooler than the upper part, attributable to the progressive heating of air along the flow direction.

For the parallel-flow and impingement-flow configurations with 60-mm fans, the maximum heat sink base temperatures are 116°C and 119°C, respectively—differing by only 2.5%. Their operational flow rates are also similar, within 5% of each other. The impingement-flow configuration with 120-mm fans demonstrates the lowest peak base temperature, at 82°C, which is 37°C lower than the other forced-convection configurations. This substantial improvement is due to its operating flow rate being approximately six times higher than that of the smaller fan configurations. The airflow in the natural convection setup is expected to remain laminar, leading to minimal mixing of fluid layers and, consequently, poor heat transfer. In contrast, forced-convection configurations generate turbulent flow, which enhances mixing through eddies and promotes efficient heat transfer by facilitating heat exchange between hot and cool fluid layers.

Junction temperatures as functions of ambient air temperature and total heat dissipation rate are shown in Fig. 7. These temperatures are calculated using Eq. (14), with the peak dissipation rate of 1200 W (400 W per IGBT module) representing the maximum load. A red dashed line in each graph indicates the maximum permissible junction temperature of 125°C [2].

Figure 7(a) shows that junction temperatures exceed the allowable limit of 125°C when natural convection is used for dissipation rates above 300 W, restricting this method to low-load IGBT operation. Similarly, Figs. 7(b) and 7(c) reveal that both the parallel-flow configuration and impingement-flow configuration with 60-mm fans cannot maintain safe junction temperatures under peak load conditions. However, Fig. 7(d) demonstrates that the impingement-flow configuration with 120-mm fans consistently keeps junction temperatures within the permissible range across all operating loads and ambient temperatures.

3.2 Liquid Cooling

Figure 8 displays the temperature distribution on the cold plate when an ethylene glycol-water solution is used as the coolant. The IGBT module locations are marked with dashed lines. In this case, the inlet coolant temperature is set to 45°C, the mass flow rate to 1.5 kg/min, and each IGBT module dissipates 300 W of heat. The coolant temperature rises by about 10°C as it passes through the cold plate. The peak temperature in the aluminum block,

located near the outlet, is 62°C significantly lower than the 119°C observed in forced air-cooling configurations. This enhanced cooling performance is attributed to the changes in flow direction at the U-turns, which disrupt the growth of the thermal boundary layer within the cold plate tube, increasing heat transfer rates.

Junction temperatures achieved with liquid cooling are plotted in Fig. 9(a) as a function of coolant mass flow rate and ambient temperature under a total dissipation rate of 1200 W. As anticipated, junction temperatures decrease with increasing coolant flow rates. Under the most challenging conditions maximum ambient temperature, minimum coolant flow rate, and maximum heat dissipation the junction temperature reaches 91°C, well below the permissible limit of 125°C. Figure 9(b) illustrates junction temperature as a function of total heat dissipation rate for different coolant flow rates, with ambient temperature fixed at 45°C. The slope of the junction temperature curve steepens as coolant flow rate decreases, indicating that the influence of flow rate adjustments becomes more pronounced at higher heat dissipation rates.

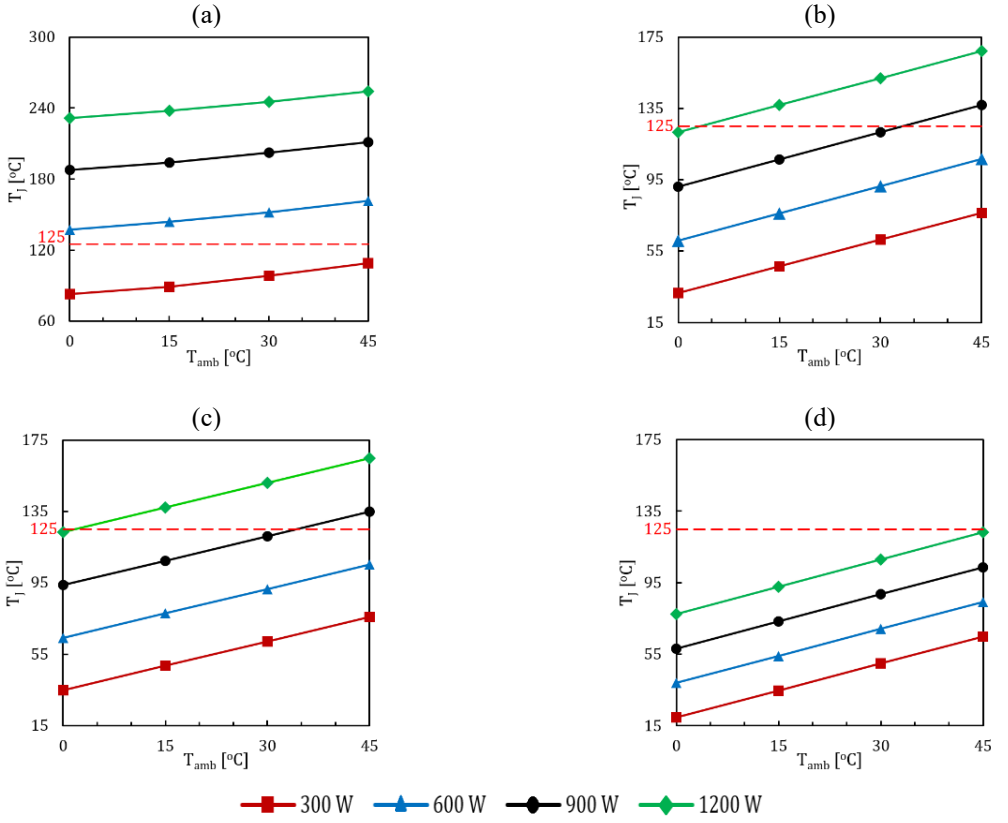

Fig. 7. Variations of junction temperature (T_J) with ambient temperature (T_{amb}) and total heat dissipation rate for (a) natural-convection, (b) forced convection with parallel-flow, (c) forced convection with impingement-flow and 60-mm fans, and (d) forced convection with impingement-flow and 120-mm fans. The maximum permissible junction temperature, which is 125°C, is indicated using a red dashed line.

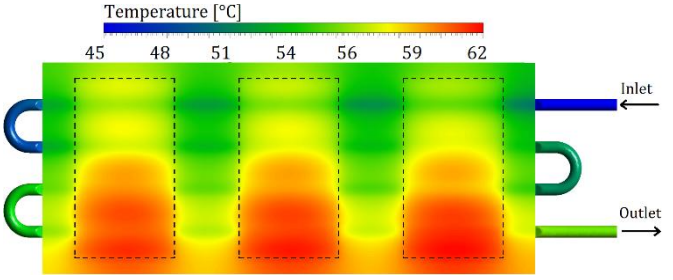

Fig. 8. Temperature distribution on the base of the liquid-cooled cold plate. To generate these plots a heat dissipation rate of 300 W for each IGBT module, ambient air temperature of 45°C and coolant flow rate of 1.5 kg/min are used. The locations of IGBT modules are depicted with dashed lines.

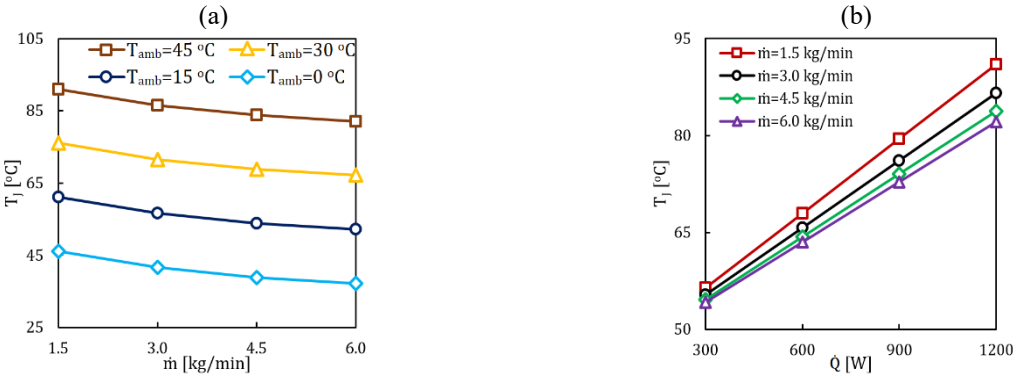

Fig. 9. Variations of (a) junction temperature with mass flow rate at a total heat dissipation rate of 1200 W, and (b) junction temperature with total heat dissipation rate for an ambient temperature of 45°C.

4. CONCLUSIONS

This study numerically evaluates the thermal management of three IGBT modules used in power inverters, comparing two conventional cooling methods: an air-cooled heat sink and a liquid-cooled cold plate. Four air-cooling configurations are analyzed: natural convection, forced convection with parallel flow, and impingement flow using two fan sizes. The junction temperatures of the IGBT modules are used as the benchmark for comparing cooling performance. A 1:1 water-ethylene glycol mixture is employed as the coolant for the liquid cooling system. Performance is assessed across a range of ambient temperatures (0°C to 45°C) and heat dissipation rates (300 W to 1200 W).

1. **Natural Convection Air Cooling**

Air cooling by natural convection is effective only for low-power dissipation rates (below approximately 300 W) and at cooler ambient temperatures. Its application is therefore limited to low-load operating conditions.

2. **Forced Convection Air Cooling (Small Fans)**

The parallel-flow configuration and impingement-flow configuration with four 60-mm fans fail to maintain IGBT junction temperatures within safe limits at high power dissipation rates and elevated ambient temperatures.

3. **High-Performance Air Cooling and Liquid Cooling**

The impingement-flow configuration with 120-mm fans and the liquid-cooled cold plate both achieve sufficient cooling to maintain safe IGBT temperatures under all tested operating conditions.

4. **Effect of Air Flow Rate and Direction**

The cooling performances of the impingement-flow configuration with 60-mm fans and the parallel-flow configuration are nearly identical at similar airflow rates, indicating that cooling efficiency is primarily influenced by airflow rate rather than airflow direction. Increasing the airflow rate with larger fans significantly reduces IGBT temperatures.

5. **Superiority of Liquid Cooling**

Liquid cooling provides a greater safety margin compared to air cooling. It keeps junction temperatures approximately 35°C below the maximum permissible limit, even under the most extreme conditions evaluated in this study.

This comparison highlights the limitations of air cooling in high-power applications and the potential of liquid cooling to offer robust and reliable thermal management.

Declaration

We acknowledge that we used ChatGPT to enhance the academic writing of our manuscript while ensuring the originality and integrity of our work.

Transparency Statement

The data supporting this study are available upon reasonable request to the corresponding author, subject to ethical and confidentiality considerations.

Acknowledgments

We would like to express our gratitude to all individuals who contributed to this project.

Declaration of Interest

The authors declare that they have no competing interests.

Funding

This research received no specific grant from any funding agency, commercial, or not-for-profit sectors.

REFRENCESS

[1] Subhedar, D. G., Chauhan, K., Panchal, S., & Bais, A. (2023). Numerical investigation of performance for liquid-cooled cylindrical electrical vehicle battery pack using Al2O3/EG-water nano coolant. *Materials Today: Proceedings*.https://doi.org/10.1016/j.matpr.2023.08.055

[2] Walters, S., Guzik, S., & Gao, X. (2018). Favre-Averaged Spatiotemporal-Filtered Large Eddy Simulation. https://doi.org/10.2514/6.2018-0373

[3] Launder, B. E., & Spalding, D. B. (1983). The numerical computation of turbulent flows. In Numerical prediction of flow, heat transfer, turbulence and combustion (pp. 96–116). Elsevier. https://doi.org/10.1016/B978-0-08-030937-8.50016-7

[4] ANSYS Inc. (2018). ANSYS Fluent User's Guide (Release 19.2). Retrieved from https://ansyshelp.ansys.com/public/Views/Secured/corp/v242/en/flu_ug/flu_ug.html

[5] Launder, B. E., & Spalding, D. B. (1972). *Lectures in mathematical models of turbulence*. Academic Press.

[6] Jonsson, H., & Moshfegh, B. (2001). Modeling of the thermal and hydraulic performance of plate fin, strip fin, and pin fin heat sinks: Influence of flow bypass. IEEE Transactions on Components and Packaging

Technologies, 24(2), 142–149. https://doi.org/10.1109/6144.926376

[7] San Ace. (2018). *DC cooling fan numbering system*. SANYO DENKI Co., Ltd.

[8] Aavid Thermalloy. (2018). Hi-Contact™ 4-Pass Cold Plate datasheet (September 2018 A02). Retrieved from https://www.mouser.com/datasheet/2/2/Hi-Contact_4-Pass_Datasheet_September_2018_A02-1487964.pdf